C. R. Geoscience 350 (2018) 476–486

Contents lists available at ScienceDirect

Comptes Rendus Geoscience

www.sciencedirect.com

Stratigraphy, Sedimentology (Palaeoenvironment)

Paleo-depths reconstruction of the last 550,000 years based on the transfer function on recent and Quaternary benthic foraminifers of the East Corsica margin

Charlie Morelle Angue Minto'O [a,b,c,*], Ricardo Silva Jacinto [d], Maria-Angela Bassetti [a,b], Gwenael Jouet [d]

[a] Université de Perpignan Via Domitia, CEFREM, UMR 5110, 52, avenue Paul-Alduy, 66860 Perpignan, France
[b] CNRS, CEFREM UMR 5110, 52, avenue Paul-Alduy, 66860 Perpignan, France
[c] École normale supérieure (ENS) de Libreville – Département des sciences de la vie et de la Terre, BP : 17009, Libreville, Gabon
[d] IFREMER, Centre Bretagne, Laboratoire "Environnements sédimentaires", 29280 Plouzané, France

ARTICLE INFO

Article history:
Received 21 September 2018
Accepted after revision 24 September 2018
Available online 23 October 2018

Handled by Vincent Courtillot

Keywords:
Benthic foraminifers
East-Corsica basin
Paleo-depths
Transfer function

ABSTRACT

In this study, the model $H(i) = 109.6103 + C_1 \times F1(i) + C_2 \times F_2(i) + \ldots + C_{33} \times F_{33}(i)$ obtained from depth modelling based on 33 recent benthic foraminifer species distribution, has been applied to the fossil benthic foraminifers from the borehole GDEC-4-2 drilled at a water depth of 491 m, in the East-Corsica basin, covering the last 550,000 years. The obtained variations of the paleo-depths show a medium correlation with the oscillations of the relative sea level and also with the fluctuations of the oxygen isotopic ratio (δ^{18}O *G. bulloides* and δ^{18}O *C. pachyderma–C. wuellerstorfi*). This newly developed transfer function is accompanied by an error margin of ± 86 m, suggesting that this model will probably be more suitable for a time scale of the order of a million years where sea level variations are recorded with larger amplitudes. Without considering these problems related to amplitudes, it also turns out that the "eustatic" signal of the microfauna is accompanied by a "trophic" signal, which should not to be neglected, especially at a millennial scale time resolution. Thus, the application of this method would require taking into account the bottom trophic effects strongly controlling the distribution of benthic foraminifer assemblages.

1. Introduction

Sea level variation reconstruction related to climatic changes are carried out using numerous tools allowing direct reading of the paleo-levels recorded by the beach rocks, the marine terraces, the coral reefs or by the evaluation of the variations of the ice volumes through the foraminifer oxygen isotopes and submerged speleothem in coastal areas (Antonioli et al., 2001; Bard et al., 1996; Chappell, 2002; Cutler et al., 2003; Rohling et al., 2009; Siddall et al., 2003). Those allowed quantifying the amplitudes related to sea level variations.

Qualitative and quantitative methods based on the microfauna assemblage distributions allowing the reconstruction of the paleo-depths are also used to characterize sea level fluctuations (Hayward, 2004; Hohenegger, 2005; Milker et al., 2011; Morigi et al., 2005; Rossi and Horton, 2009; Spezzaferri and Tamburini, 2007). These methods are based on a very good knowledge of the distribution of living foraminifera and on the assumption that the ecological requirements of specific *taxa* have not changed over time. In this study, we use this principle to establish a

* Corresponding author. Université de Perpignan Via Domitia, CEFREM, UMR 5110, 52, avenue Paul-Alduy, 66860 Perpignan, France.
E-mail addresses: mintoocharly@yahoo.fr, charlie.angue-mintoo@univ-perp.fr (C.M. Angue Minto'O).

https://doi.org/10.1016/j.crte.2018.09.003

transfer function in which the recent benthic foraminifer assemblages of the East-Corsican margin are used for modelling the depths according to the formula: $H_{m,j} = a_{c,0} + Z_{j,k} \cdot a_{c,k}$, where $H_{m,j}$ is the modelled depth at each site j, $Z_{j,k}$ is the matrix containing the values of the principal components used in the model. Each line (j) is associated with a site; each column k is associated with an used principal component. Both the scalar $a_{c,0}$ and the vector $a_{c,k}$ are estimated by calibration based on least-squares interpolation.

The level of correlation observed between these modelled depths and the actual depths will allow the application of this equation to fossil benthic foraminifer assemblages. Comparison with other eustatic curves will allow discussing this method of sea level reconstruction and evaluating the difficulties of using benthic assemblages as tools of variations in the water column.

2. Study area

Located in the northern part of the Tyrrhenian Sea (Western Mediterranean), the East-Corsica margin is a continental shelf region varying from 5 to 10 km in width in the northern part to 25 km in the southern one. The continental shelf characterizing the East-Corsica margin is narrow, with a shelf break situated around 110–120 m (Gervais, 2002; Gervais et al., 2004). This continental shelf is followed by a steep continental slope incised by numerous meandering canyons (Gervais, 2002). The latter open out into a deep basin, which is characterized by a depression named Corsican Trough.

3. Materials and methods

3.1. Micropaleontological and stable isotope analyses

Before performing micropaleontological analyses, samples were washed and sieved (63 μm) on the sedimentary fraction > 150 μm. The recent benthic foraminifers of the East-Corsica basin were studied in 45 surface samples from the interface cores collected at depths ranging from 7 to 868 m, and 101 benthic foraminifer *taxa* were identified (Angue Minto'o et al., 2013). The identification of 84 *taxa* of fossil benthic foraminifer was possible via the analysis of 291 samples from the GDEC-4 borehole drilled at a water depth of 492 m in the East-Corsica margin covering the last 550,000 years (Angue Minto'o et al., 2016).

Oxygen stable isotope measurements were performed on specimens of planktonic foraminifera species *Globigerina bulloides* and *G. ruber* (white) from the 250–315 μm size fraction, *Neogloboquadrina pachyderm*a (dextral) from the 200–250 μm size fraction, and on the epifaunal benthic foraminifera *Cibicides wuellerstorfi*, *Cibicidoides pachyderma* and *Cibicidoides kullenbergi* found in the > 150 μm size fraction (Toucanne et al., 2015).

3.2. Species selection and principal component analysis

In this study, MatLab generic functions are used for the computations. We call $M_0(i,j)$, the initial matrix of species to be consider in the analysis. $M_0(i,j)$ consists of relative abundances of the all benthic foraminifers (101 species) identified in the surface samples, where i is the site and j the species. With the aim of obtaining qualitative results, the reduction of the number of species of $M_0(i,j)$ is made by eliminating species with a median equal to 0. Because Principal Component Analysis (PCA) is based on correlation analysis and hence variation quantifications, consequently, on 101 recent benthic foraminifer taxa identified, only 33 taxa were retained and are listed in Table 1. For these 33 species, the relative abundance, at one site, is always calculated using the total number of individuals per site based on the 101 species. This allowed maintaining independence between the frequencies retained, i.e. the sum of the species frequencies per site does not equal 1, and the dependent and untreated variable is "the other species"

$$\sum_{j=1}^{33} M_{ij \leq 1}$$

where M is the abundance matrix of site i and of species j. The analysis is based on the abundance matrix M expressing at each site i (from 1 to ***) the abundance of each species j (from 1 to 33). Each value of M is hence expressed by M_{ij}.

Table 1
Presentation of the 33 benthic foraminifers derived from the analysis of the interface samples and having a median greater than 0. These 33 taxa were selected for the principal component analysis.

Retained species	Order number
Amphicoryna scalaris	1
Bulimina marginata	2
Bulimina costata	3
Bigenerina nodosaria	4
Biloculinella labiata	5
Bolivina spathulata	6
Cibicides wuellerstorfi	7
Cibicides lobatulus	8
Cibicides sp.	9
Cyclogyra carinata	10
Cassidulina carinata	11
Cassidulina crassa	12
Cassidulina minuta	13
Elphidium macelum	14
Fissurina cucullata	15
Gyroidina orbicularis	16
Gyroidina altiformis	17
Hoeglundina elegans	18
Hyalinea balthica	19
Lenticulina sp.	20
Melonis barleeanus	21
Pseudoclavulina crustata	22
Quinqueloculina duthiersi	23
Quinqueloculina viennensis	24
Quinqueloculina seminulum	25
Rosalina globularis	26
Spiroloculina escavata	27
Sigmoilopsis schlumbergeri	28
Spiroplectinella sagitula	29
Textularia agglutinans	30
Textularia truncata	31
Valvulinaria bradyana	32
Uvigerina mediterranea	33

PCA is based on the covariance matrix (M_c) estimated on the basis of the species abundance matrix by site:

$$M_{c,kj} = \mathrm{cov}(M_{ij}, M_{ik})$$

$M_{c,kj}$ represents the correlation between species k and j for the all sites i: $M_{c,kj} = M_{c,jk}$.

The eigenvalues and eigenvectors of the matrix M_c are computed to establish, respectively, the weight (variance) associated with each component and the coefficients of the principal components. Thus, the matrix of the eigenvectors C_{jk}, and the coefficients of the principal components are calculated as well as the diagonal matrix of the eigenvalues D_{jk}. The new matrix C_{jk} verifies the following equality:

$$M_{c,kj} \cdot C_{jk} = C_{jk} \cdot D_{jk}$$

The principal components are obtained by a "rotation" of the assembly matrix (M_{ij}) along the principal vectors described by the matrix of eigenvectors or coefficients of the components

$$Z_{ik} = M_{ij} \cdot C_{jk}$$

It is important to keep in mind that the matrix Z_{ik} contains the same amount of information as the initial abundance matrix M_{ij} from which Z_{ik} has been derived. The information is organised in a new way, the components being independent of one another. Hence, at each site i, Z_{ik} provides the local value of component k, while M_{ij} provides the local abundance of species j, the number of species and of components being the same (33).

The matrix C_{jk} co-relates the principal components and the species. Even if it is computed from the data, it contains an estimation of a relation that is supposed to be valid for any assemblage (not only the ones in the data). C_{jk} is the same for all sites (observed or noted) and is the base of the generalization.

At each new site,

$$H_k = a \cdot Z_k + b = a \cdot C_{kj} \cdot M_j + b$$

We can evaluate the possibility of obtaining a model linking the species assemblages and the depth of the sites.

3.3. One-component models

For each component Z_k, one can define a depth model H_k obtained by linear regression for the depth H:

$$H_k = a \cdot Z_k + b$$

where the coefficients a and b are estimated by the least squares method for each component. Thus a function B_k can be defined. This function gives the correlation level (coefficient) obtained by regression (R) between the modelled depth H_k and the true depth H.

$$B_k = R(H_k, H)$$

3.4. Multi-component models

For models consisting of several components, the method applied is the same. A depth model is obtained by linear regression using the least squares method. Here the most representative component of the variance is used. Thus, a depth model H_n can be defined, where n is the number of components used (from the highest to the lowest):

$$H_n = a_0 + \sum_{k-1}^{n} a_{ij} \cdot Z_k$$

The performance of the model H_n can be associated with the A_n function,

$$A_n = R(H_n, H)$$

The value A_6 will give the correlation level of a regression model based on the six most important components in terms of assemblage variability.

3.5. Determination of the freedom factor

A freedom factor (λ_n) of a model consisting of principal components n with respect to the points number (P) of calibration/validation is defined by the following formula:

$$\lambda_n = \frac{P-(n+1)}{P}$$

A freedom factor is defined to quantify the robustness of the models based on the number of its number of freedom degrees. For a model based on n principal components, its freedom factor (L_n) is quantified by the number of data points used for calibration (P) and the number of degrees of freedom of the used model ($n+1$, if n PCs are used).

If this factor is close to the unit, the model is robust in terms of degrees of freedom. If the factor is close to zero, the model is not robust, and there are too many degrees of freedom compared to the size of the data available and the basis of its construction. In our study, $P = 44$.

An performance indicator of the model could be defined as the "good" compromise between the correlation level and its performance or factor of freedom. The quality of a model H_n described by the function Q_n is defined as follows:

$$Q_n = R(H_n, H) \cdot \lambda_n = A_n \cdot \lambda_n$$

3.6. Calibration and validation of the models

After a ranking based on their depths, the 44 sites are divided into two groups. The first one is composed of one

site out of two and it is called "calibration". This group includes variables with an index c. The second group consists of the other sites and it is called "validation". This validation group is characterized by variables with an index v. The coefficients a_k are calculated by regression on the basis of the following system of equations:

$$a_0 + Z_{ik} \cdot a_k = H_i$$

The modelled values will then be:

$$H_{m,i} = a_0 + Z_{i,k} \cdot a_k$$

where a_k represents the regression coefficients estimated by the least squares method and Z_{ik} represents the principal component value k at site i. H_i is the true depth at site i and $H_{m,i}$ represents the depth modelled at point i. As we have 22 sites for calibration and validation, it is clear that the number of components must be well below this number (we tested from one to six components). The real model is based on calibration data (i.e. sites). The associated coefficients are thus obtained:

$$a_{c,0} + Z_{c,k} \cdot a_{c,k} = H_c$$

The calibration coefficients are then used for the validation data in order to obtain the simulated data $H_{m,v}$:

$$H_{m,j} = a_{c,0} + Z_{jk} \cdot a_{c,k}$$

4. Results and discussion

4.1. Principal component analysis (PCA)

The results of the PCA show that a very important part of the variance (> 90%) is contained in the first five eigenvalues, or principal components (Fig. 1). The contribution of each species to the two main components can be visualized by the respective contributions of each species (Fig. 2). It may be noted in Fig. 2 that the species that contribute the most to the expression of the first component are *M. barleeanus* (21) and *U. mediterranea* (33). This component is modulated (attenuated) by the presence of *C. carinata* (11), *R. globularis* (26), and *Q. duthiersi* (23). The second component, however, is expressed by the "competition" between *C. carinata* and *R. globularis* (Fig. 2).

4.2. Correlation between depths and principal components

The correlation levels between the depth of the sites and the principal components associated with the assemblages are presented in Fig. 3. The function B is represented by the blue bars that indicate the correlation level of each component with the depth. The function A is represented by the red curve. This latter indicates the correlation level reached by regression between a set of N components and the depth. Thus, the component 33, which is the first in importance, is the one that shows the best correlation with the depth. This component alone allows having a correlation level higher than 95% (Fig. 3). The other components are individually weaker. However, they allow increasing the total correlation to more than 99% if all 33 components are used to reproduce the 44 depths.

The best model is not necessarily the one that allows obtaining the best correlation between true values and model values estimated on these same true values. The number of degrees of freedom associated with the calibrated models and the number of validation points must be taken into account, because the models are calibrated on the validation points. Thus, all models H_k have two degrees of freedom: the coefficients a and b. The models H_n have $n + 1$ degrees of freedom. By absurdity, a model whose number of degrees of freedom is equal to the number of calibration/validation points will always present a correlation of 100%.

The representation of the function Q_n (Fig. 4) shows that the use of a small number of components can be advantageous in terms of robustness of the chosen model.

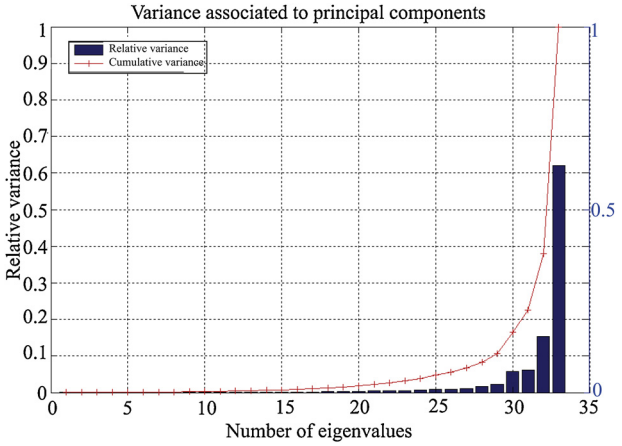

Fig. 1. Variance associated with the 33 main components. The majority of the variance is contained in the first five eigenvalues, or principal components.

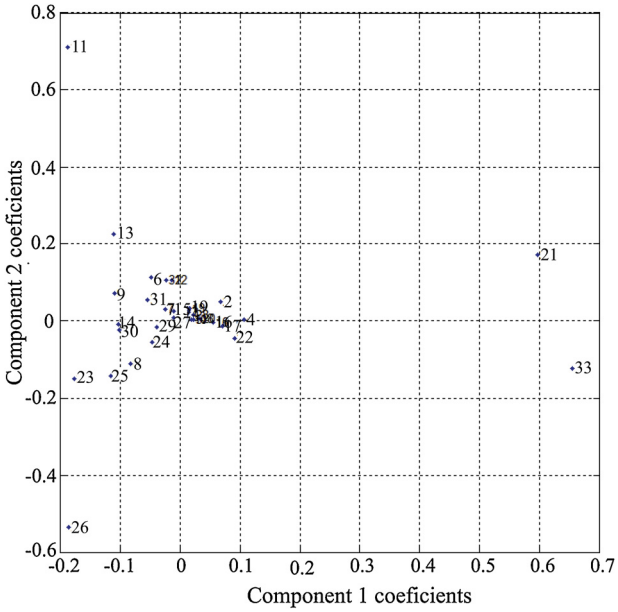

Fig. 2. Species contribution to the two main components.

4.3. Evaluation of the models

The evaluation is made for models built with a number of variable components (between 1 and 6). The model with all the data (blue curve) serves as a reference (Fig. 5). Calibration 1 (cal 1) and validation 1 (val 1) are obtained as described in the paragraph related to calibration and validation of models: the first set is for calibration and the second set for validation. The models cal. 2 and val. 2 are obtained by reversing the use of the sets (Fig. 5).

For cal. and val. 1, we obtain a calibration model that is slightly less efficient than the reference one, while the validation is generally better (Fig. 5). This means that the validation set is closer, in terms of assemblages, to what can be explained by the depth. Overall, the correlation improves with the number of components used. This improvement is increasing for the reference and for the calibration (Fig. 5). For the validation model, the two minor contribution components (2 and 5) reduce the performance of the model. When we reverse the use of sets, we fall back on a reverse result, and more "classic". Calibration, done on less data than the reference, is more efficient (but with a lower freedom factor); validation is less well than calibration and reference.

The choice seems to be made between 1, 4, or 6 components, even if it remains conceivable to use only the useful components. Correlations are performance indicators. It is therefore important to visualize the

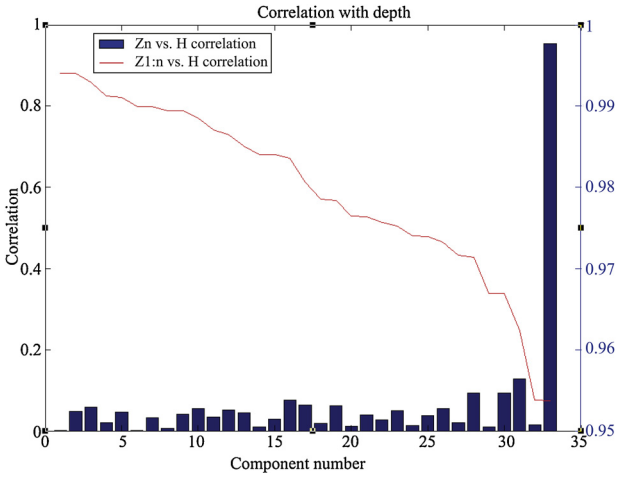

Fig. 3. Correlation between the depth of the sites and the principal components. The blue bars represent the function B and the red curve characterizes the function A.

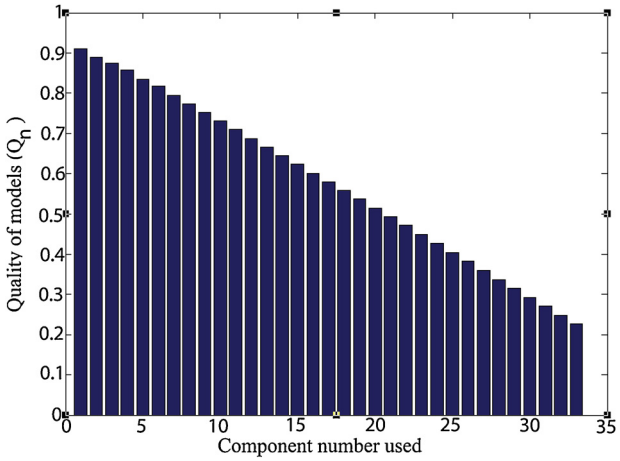

Fig. 4. Representation of the function Q_n.

correlations presented in Figs. 6 and 7, in which a loss of linearity can be observed from 700 m depth with the error margins of 43 m and thus 86 m in 2σ.

4.4. Choice of the final model

Principal component analysis allows us to "focus" the variance of the assemblages on a very small number of variables (components), which is very useful in order to reduce the number of freedom degrees of the models obtained by regression.

Out of 33 components (as much as the selected species), we will keep four components (28, 30, 31 and 33), which means that the regression model is based on the estimation of five parameters.

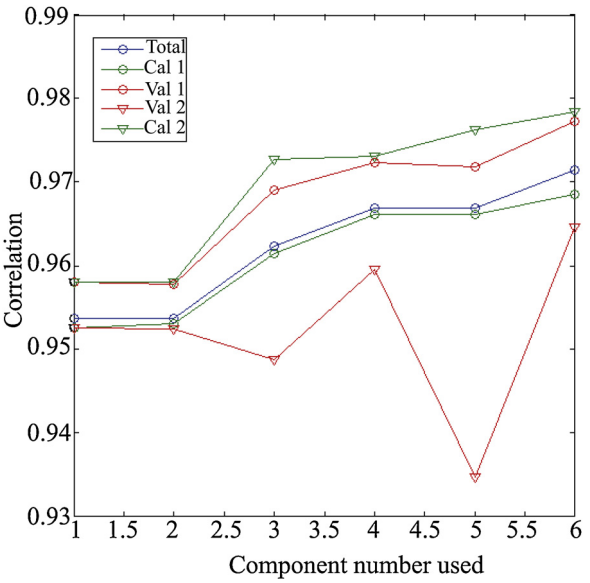

Fig. 5. Evaluation of the different models: the one with all the data (blue curve) and the models calibration (green curves) and validation (orange curves).

The model obtained made it possible to have a 97.13% correlation on all the sites. The calibrated model on 22 sites (performance of 96.85% in self-application) displays a correlation of 97.72% on the validation set. The performance of the chosen model is illustrated in the Fig. 8.

4.5. The structure of the model

The structure of the model is presented in Fig. 9. It can be noted that the final contribution to explaining the depth variability is very distinct from the distribution of the coefficients associated with each species. This is because the relative abundance of each species has not been standardized. Thus, there are two species that contribute significantly: *M. barleeanus* and *U. mediterranea*. *M. barleeanus* explains the variations of depth at shallow depths and *U. mediterranea* explains the depth beyond 100 m.

4.6. Application of the model and comparison with the semi-quantitative method

4.6.1. Numerical model

The application of the model $H(i) = 109.6103 + C_1 \times F1(i) + C_2 \times F_2(i) + \ldots + C_{33} \times F_{33}(i)$ (where C_i corresponds to the coefficient of species i and F_i to its frequency) on fossil benthic foraminifers species allowed us to obtain the curve of paleo-depths variation. The reconstructed paleo-depths range from 622 ± 86 m to 21 ± 86 m. In general, the variation of these paleo-depths correlates quite well with the variations of the sea level (Fig. 10). A global trend marked by an increase in depth during periods of high sea level is observed. Interglacials are characterized by the removal (or melting) of glaciers that conduct to an increase in sea level (Dorale et al., 2010) and therefore to an increase in the water level above the seabed. This could justify this rise of the paleo-depths during these warm climatic periods. However, these paleo-depth variations are characterized by very large amplitudes.

Based on the fact that these modelled amplitudes are affected by (1) local effects related to the morphology of

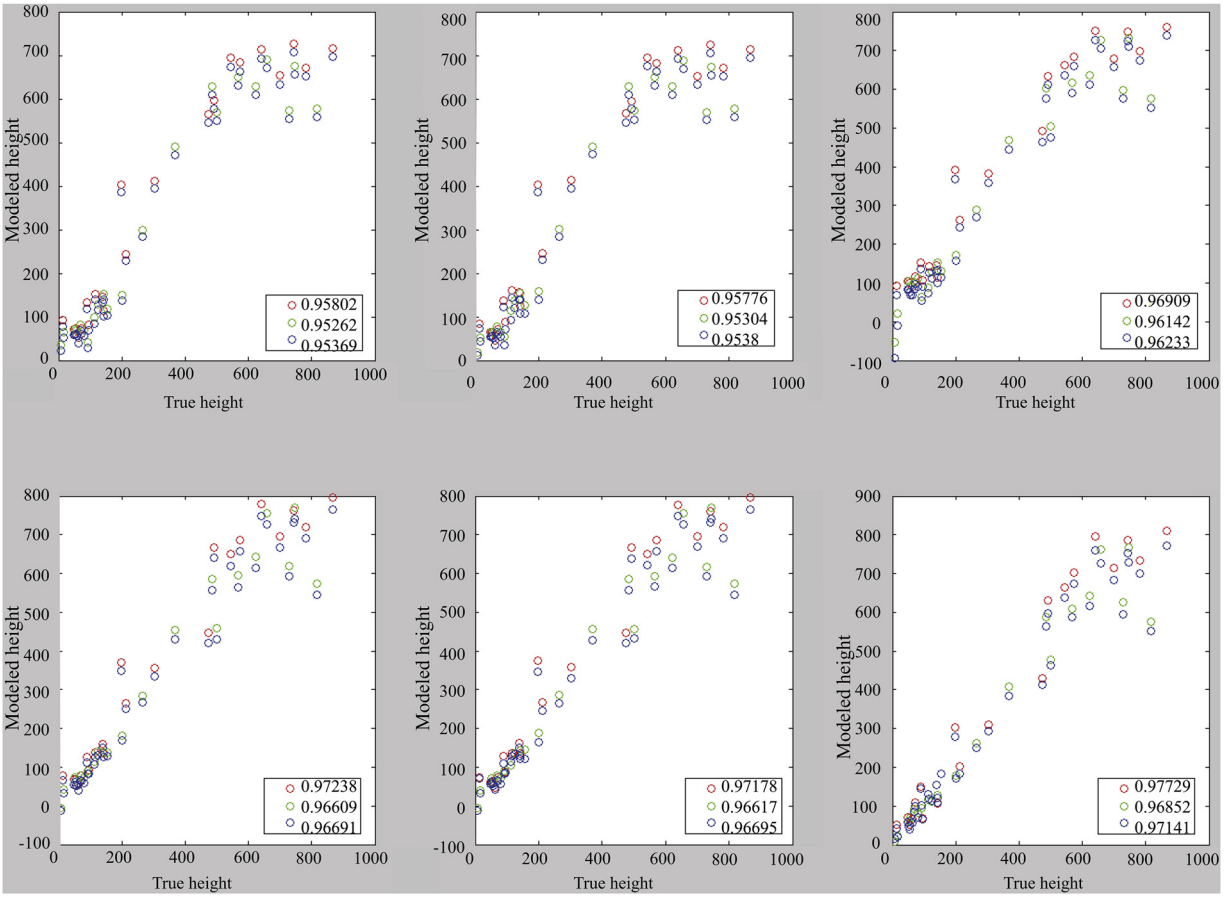

Fig. 6. Correlation for models with the use of one to six main components (from top left to bottom right). Calibration set: cal. 1. Reference (blue), calibration (green), and validation (red).

the basin, which is shallow and semi-marine (close to the sources), (2) changes in trophic conditions at the bottom strongly influencing the variations of benthic microfauna assemblages, (3) uncertainties related to the calculation method and the bathymetry. Normalization from 0 to 120 m was thus made on the values of paleo-depths and the sea level variation curve obtained was compared with the eustatic curve established by Rohling et al. (2009) and smoothed in the same way (Fig. 11). This results in a fairly good correlation between these two curves.

However, very large temporal offsets in amplitude and in time are observed between the two interglacial curves: between 290 and 280,000 years (15 ka), 200 and 180,000 years (15 ka), 170 and 160,000 years (15 ka), 125 and 100,000 years (30 ka) and between 60 and 30,000 years (30 ka, Fig. 11).

These offsets therefore appear during periods of high sea level that are globally characterized by a decrease in the organic matter inputs related to the theoretical distance of the sources (Cortina et al., 2013) and by a decrease in the ventilation at the sea bottom (Toucanne et al., 2012). The offsets result from an underestimation of the depths that could be related to the non-integration in the model of the changes in bottom trophic conditions strongly influencing the variations of benthos foraminifer assemblages (De Rijk et al., 2000; Fontanier et al., 2002; Gooday, 2003; Jorissen et al., 1995; Mackensen et al., 1990; Murray, 1991; Schönfeld, 2002a; Schönfeld, 2002b). Indeed, *U. mediterranea* and *M. barleeanus* are the two species of benthic foraminifers that strongly influence the calculation of paleo-depth. This is illustrated by the perfect correlation between the normalized eustatic variation curve and the variation in their cumulative abundance curve (Fig. 11). *U. mediterranea and M. barleeanus* are species related not only to the quality but also to the intensity of organic matter inputs to the bottom. *M. barleeanus* is known as a species that develops in environments where there is the refractory organic matter (Fontanier et al., 2002; Lutze and Coulbourn, 1984) and *U. mediterranea* adapts to environments with moderate fluxes of labile organic matter (Lutze and Coulbourn, 1984; Schmiedl et al., 2000).

Based on this low correlation and the error margins obtained (± 86 m), and on the significant offsets observed with the relative sea level variation curve (15 and 30 ka), we can say that on a time scale of 100,000 years, the method is difficult to apply. Because at this time scale, the variation amplitudes of the sea level (the order of one hundred meters) remain lower compared to the margin of error (± 86 m) applied to our model. The transfer function could therefore be

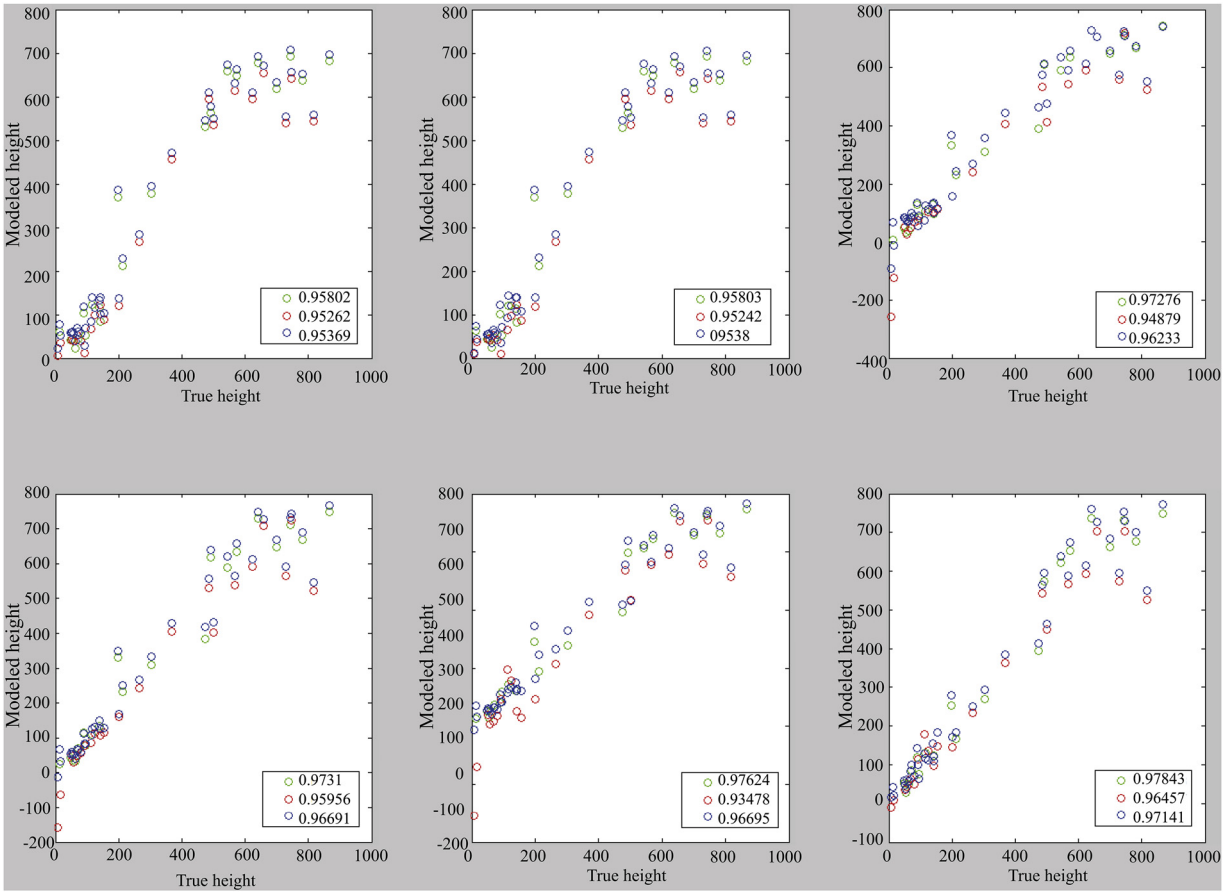

Fig. 7. Correlation for models with the use of one to six main components (from top left to bottom right). Calibration set: cal. 2. Reference (blue), calibration (green) and validation (red).

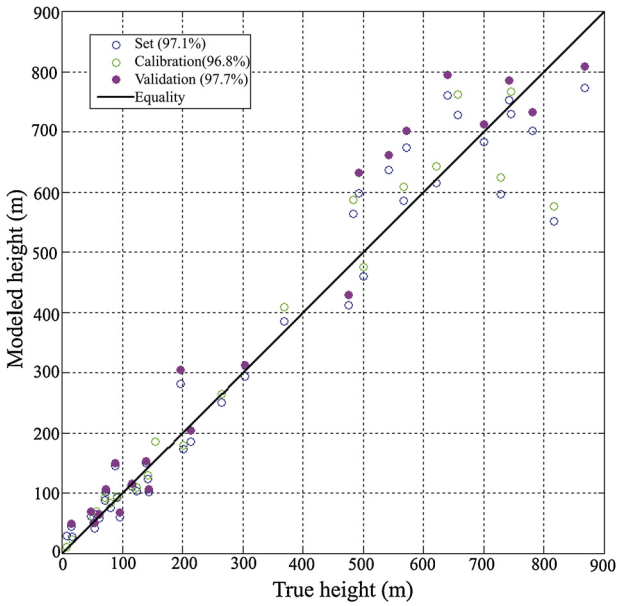

Fig. 8. Performance of the selected model: correlation between "true" depths and modelled depths.

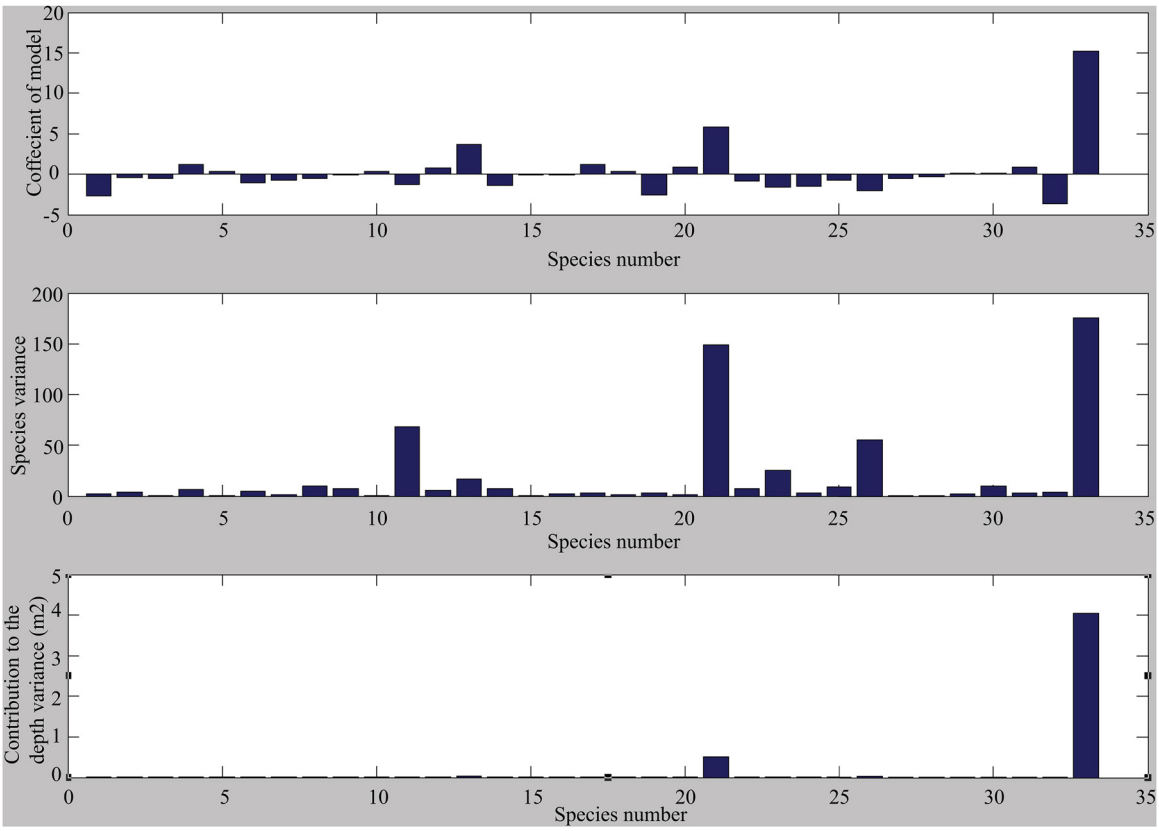

Fig. 9. Model structure: coefficients and variance per species.

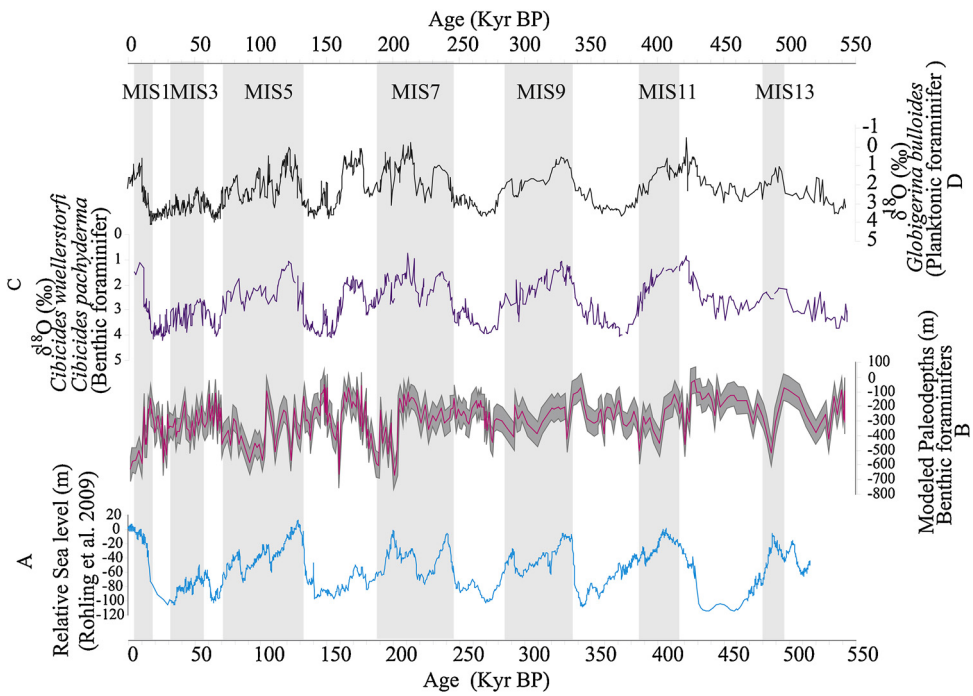

Fig. 10. Characterization of the paleo-depth variation during the last 500,000 years. Comparison between: A, the relative sea level variation curve (Rohling et al., 2009); B, the curve of variation of the modelled paleo-depths; C and D, curves of changes in oxygen isotopic ratio of benthic (*Cibicides wuellerstofi* and *Cibicides pachyderma*) and planktonic (*Globigerina bulloides*) foraminifers.

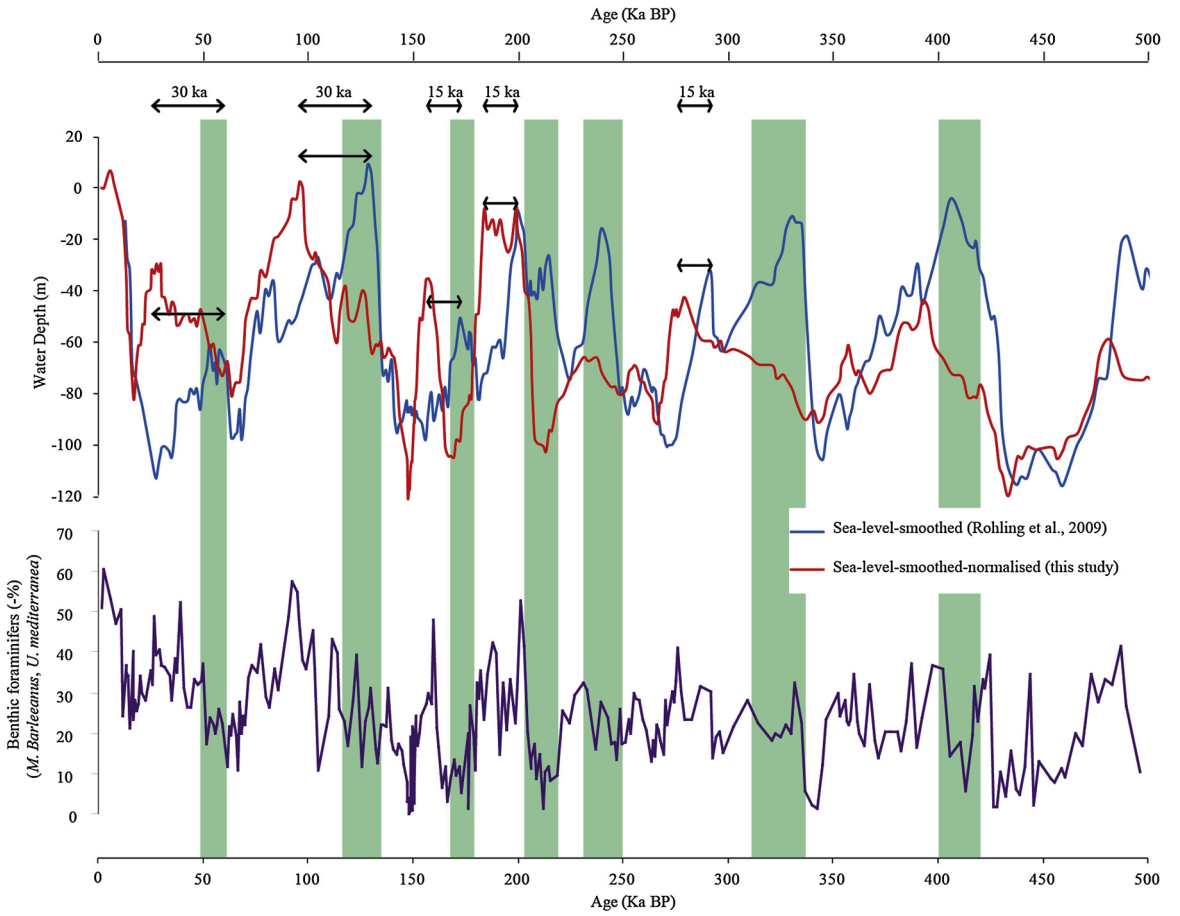

Fig. 11. Standardized and smoothed sea level variation curve compared with the smoothed sea level variation curve from Rohling et al. (2009) and the relative abundance variation of benthic foraminifers *Melonis barleeanus* and *Uvigerina mediterranea*. A good correlation is observed between normalized eustatic variations and abundance variations of *Melonis barleeanus*/*Uvigerina mediterranea*. A significant shift during periods of high sea level is observed between the two eustatic curves.

more suitable on a million-year time scale in which sea level variations are recorded with larger amplitudes and where isotopes are difficult to use.

5. Conclusion

Depth modelling using 33 species of recent benthic foraminifers in the East Corsica margin was based on a principal component analysis (PCA) that allows us to obtain the model $H(i) = 109.6103 + C_1 \times F1(i) + C_2 \times F_2(i) + \ldots + C_{33} \times F_{33}(i)$ with a correlation of 97.1%. The application of this model on fossil benthic foraminifers conducts to the establishment of a paleo-depth variation curve with a margin of error of $\pm$ 86 m. The resulting sea-level variation curve shows significant shifts during high sea levels, which could partly be explained by the significant evolution of trophic conditions during interglacial periods. This margin of error and this offset can be indicators of the limit of application of this transfer function on a scale of 100,000 years where the sea level variation amplitudes are in the order of a hundred meters. On the other hand, on a million-year scale that is characterized by variation with larger amplitudes, this model could provide an interesting estimation. In order to reduce the margin of error and to avoid a significant signal disturbance, it is necessary to take into account, in the function of transfer, the environmental parameters, in particular the concentration and quality of the organic matter and other nutrients that largely affect the bathymetric distribution of benthic foraminifers.

This paper is invited in the frame of the 2017 Prizes of the French Academy of Sciences (“bourse Louis-Gentil de l’Académie des sciences”). Il has been reviewed by Philippe Janvier, Dominique Gibert, and Vincent Courtillot.

Supplementary data associated with this article can be found, in the online version, at https://doi.org.10.1016/j.crte.2018.09.003.

References

Angue Minto'o, C.M., Bassetti, M.A., Jouet, G., Toucanne, S., 2013. Distribution of modern ostracods and benthic foraminifers from the Golo margin (East-Corsica). In Colin, J.-P., Sauvagnat. 27e Réunion des ostracodologistes de langue française (ROLF) en l'honneur de H.J Oertli, 1–3 juin 2012. Rev. Paléobiol. 32 (2), 607–628.

Angue Minto'o, C.M., Bassetti, M.-A., Toucanne, S., Jouet, G., 2016. Distribution of ostracod and benthic foraminiferal assemblages during the last 550 kyr in the East-Corsica basin, western Mediterranean Sea: A paleo-environmental reconstruction. Rev. Micropaléontol. 59 , http://dx.doi.org/10.1016/j.revmic.2016.01.002.

Antonioli, F., Silenzi, S., Frisia, S., 2001. Tyrrhenian Holocene palaeoclimate trends from spelean serpulids. Quat. Sci. Rev. 20, 1661–1670.

Bard, E., Hamelin, B., Arnold, M., Montaggioni, L., Cabioch, G., Faure, G., Rougerie, F., 1996. Deglacial sea-level record from Tahiti corals and the timing of global meltwater discharge. Nature 382, 241–244.

Chappell, J., 2002. Sea level changes forced ice breakouts in the Last Glacial cycle: new results from coral terraces. Quat. Sci. Rev. 21, 1229–1240.

Cortina, A., Sierro, F.J., Filippelli, G., Flores, J.A., Berné, S., 2013. Changes in planktic and benthic foraminifer assemblages in the Gulf of Lions, off south France: Response to climate and sea level change from MIS 6 to MIS 11. Geochem. Geophys. Geosyst. 14, 1258–1276.

Cutler, K.B., Edwards, R.L., Taylor, F.W., Cheng, H., Adkins, J., Gallup, C.D., Cutler, P.M., Burr, G.S., Bloom, A.L., 2003. Rapid sea-level fall and deep-ocean temperature change since the last interglacial period Earth Planet. Sci. Lett. 206, 253–271.

De Rijk, S., Jorissen, F.J., Rohling, E.J., Troelstra, S.R., 2000. Organic flux control on bathymetric zonation of Mediterranean benthic foraminifera. Mar. Micropaleontol. 40, 151–166.

Dorale, J.A., Onac, B.P., Fornós, J.J., Ginés, J., Ginés, A., Tuccimei, P., Peate, D.W., 2010. Sea-Level Highstand 81,000 Years Ago in Mallorca. Science 327, 860–863.

Fontanier, C., Jorissen, F.J., Licari, L., Alexandre, A., Anschutz, P., Carbonel, P., 2002. Live benthic foraminiferal faunas from the Bay of Biscay: faunal density, composition, and microhabitats. Deep Sea Res. Part 1 Oceanogr. Res. Pap. 49, 751–785.

Gervais, A., 2002. Analyse multi-échelles de la morphologie, de la géométrie et de l'architecture d'un système turbiditique sableux profond (système du Golo marge est-Corse, mer Méditerranée), 1. Université de Bordeaux, France, 315 p.

Gervais, A., Savoye, B., Mulder, T., Piper, D.J.W., Cremer, M., Pichevin, L., 2004. Present morphology and depositional architecture of a sandy sub-marine system: the Golo turbidite system (Eastern margin of Corsica). In: Joseph, P., Lomas, S.A. (Eds.), Confined turbidite systems. Geological Society, London, pp. 59–89.

Gooday, A.J., 2003. Benthic foraminifera (Protista) as tools in deep-water palaeoceanography: environmental influences on faunal characteristics. In: Southward, A.J., Tyler, P.A., Young, C.M., Fuiman, L.A. (Eds.), Advances in Marine Biology, 46, Academic Press, London, pp. 3–90.

Hayward, B.W., 2004. Foraminifera-based estimates of paleobathymetry using Modern Analogue Technique, and the subsidence history of the early Miocene Waitemata Basin. New Zealand J. Geology and Geophysics 47, 749–767.

Hohenegger, J., 2005. Estimation of environmental paleogradient values based on presence/absence data: a case study using benthic foraminifera for paleodepth estimation. Palaeogeogr. Palaeoclimatol. Palaeoecol. 217, 115–130.

Jorissen, F.J., de Stigter, H.C., Vidmark, J.V., 1995. A conceptual model explaining benthic foraminiferal microhabitats. Mar. Micropaleontol. 26, 3–15.

Lutze, G.F., Coulbourn, W.T., 1984. Recent benthic foraminifera from the continental margin of northwest Africa: Community structure and distribution. Mar. Micropaleontol. 8 (5), 361–401.

Mackensen, A., Grobe, H., Kuhn, G., Fütterer, D., 1990. Benthic foraminiferal assemblages from the eastern Weddell Sea between 68 and 73°S: Distribution, ecology and fossilization potential. Mar. Micropaleontol. 16, 241–283.

Milker, Y., Schmiedl, G., Betzler, C., 2011. Paleobathymetric history of the Western Mediterranean Sea shelf during the latest glacial period and the Holocene: Quantitative reconstructions based on foraminiferal transfer functions. Palaeogeogr. Palaeoclimatol. Palaeoecol. 307, 324–338.

Morigi, C., Jorissen, F.J., Fraticelli, S., Horton, B.P., Principi, M., Sabbatini, A., Capotondi, L., Curzi, P.V., Negri, A., 2005. Benthic foraminiferal evidence for the formation of the Holocene mud-belt and bathymetrical evolution in the central Adriatic Sea. Mar. Micropaleontol. 57, 25–49.

Murray, J.W., 1991. Ecology and Palaeoecology of Benthic Foraminifera. Longman, Scientific and Technical, London, 397 p.

Rohling, E.J., Grant, K., Bolshaw, M., Roberts, A.P., Siddall, M., Hemleben, C., Kucera, M., 2009. Antarctic temperature and global sea level closely coupled over the past five glacial cycles. Nature Geosci advanced online publication. .

Rossi, V., Horton, B.P., 2009. The application of subtidal foraminifera-based transfer function to reconstruct Holocene paleobathymetry of the Po Delta, northern Adriatic Sea. J. Foraminiferal Res. 39 (3), 180–190.

Schmiedl, G., de Bovée, F., Buscail, R., Charrière, B., Hemleben, C., Medernach, L., Picon, P., 2000. Trophic control of benthic foraminiferal abundance and microhabitat in the bathyal Gulf of Lions, western Mediterranean Sea. Mar. Micropaleontol. 40, 167–188.

Schönfeld, J., 2002a. Recent benthic foraminiferal assemblages in deep high-energy environments from the Gulf of Cadiz (Spain). Mar. Micropaleontol. 44 (3–4), 141–162.

Schönfeld, J., 2002b. A new benthic foraminiferal proxy for near-bottom current velocities in the Gulf of Cadiz, northeastern Atlantic Ocean. Deep Sea Res. Part 1 Oceanogr. Res. Pap. 49 (10), 1853–1875.

Siddall, M., Rohling, E.J., Almogi-Labin, A., Hemleben, C., Meischner, D., Schmelzer, I., Smeed, D.A., 2003. Sea-level fluctuations during the last glacial cycle. Nature 423, 853–858.

Spezzaferri, S., Tamburini, F., 2007. Paleodepth variations on the Eratosthenes Seamount (Eastern Mediterranean): sea-level changes or subsidence? eEarth Discussions 2, 115–132.

Toucanne, S., Jouet, G., Ducassou, E., Bassetti, M.A., Dennielou, B., Angue Minto'o, C.M., Touyet, N., Charlier, K., Lericolais, G., Mulder, T., 2012. A 130,000-year record of Levantine Intermediate Water flow variability in the Corsica Trough, Western Mediterranean Sea. Quat. Sci. Rev. 33, 55–73.

Toucanne, S., Angue, MintoC.M., Fontanier, C., Bassetti, M.-A., Jorry, S.J., Jouet, G., 2015. Tracking rainfall in the northern Mediterranean borderlands during sapropel deposition. Quat. Sci. Rev. 129, 178–195.